Performance of the GSN station XAN-IC, 1992-2009

A report in a series documenting the status of the Global Seismographic Network

WQC Report 2010:4
January 17, 2010

Göran Ekström and Meredith Nettles

Waveform Quality Center
Lamont-Doherty Earth Observatory of Columbia University, New York

1 Station performance report: XAN

This report summarizes a number of observations that are relevant for assessing the past and current quality of the data recorded at one of the stations of the Global Seismographic Network. The purpose of the report is, in part, to document specific problems observed with the data. Some of these problems are related to errors in the available descriptions of station parameters: orientation of the sensors, response functions, polarities. In principle, such errors in the station metadata can be corrected by providing updated station parameters. In practice, this may be difficult in some cases due to lack of knowledge of, or inability to determine, the correct parameters. Other problems are caused by the malfunctioning of some instrument component. Regardless of the cause, it is necessary to document and publicize the lack of accurate and reliable station characteristics, especially when it is not obvious from simple inspection of the data that a problem exists. It is also of value to document the characteristics of stations performing well, both to establish their high quality and to help identify installation and operation procedures that should be emulated at other stations.

1.1 Station XAN

The station XAN (Xi'an) is located at the outskirts of the city Xi'an in the Shaanxi province of central China (Figure 1). It is $\sim$400 km distant from a mountainous and seismically active region to the southwest. The closest GSN station is ENH (Enshi), located approximately 500 km to the south.

XAN is part of the New China Digital Seismic Network (network code IC) and is maintained by the USGS.

1.2 The data

Digital seismic data from XAN are available from the IRIS DMC beginning in 1992. Here, we consider broadband instruments at the station. The initial installation consisted of an STS-2 seismometer. A set of STS-1 seismometers was installed in 1995, after which time the STS-2 can be considered auxiliary. Data from XAN are included in our standard CMT analysis (Dziewonski et al., 1981; Ekström et al., 2005), and waveform data, travel-time observations, and dispersion curves derived from XAN data have been used in the development of numerous global and regional tomographic models since the station was installed. It is also an important station for nuclear-monitoring activities.

In the analyses described here, we have made use of data collected from the IRIS DMC. We requested and downloaded all long-period (LH) and very-long-period (VH) data available at the DMC for both sensors from the start of operation (1992) until August 2009. We used the currently available station metadata prepared by the Albuquerque Seismological Laboratory and available at the IRIS DMC (downloaded in December 2009). Overall, the station has been operated with few data outages since 1992.

1.3 The metadata

The dataless SEED volume for XAN documents 3 response epochs for the STS-1 (primary) and STS-2 (initially primary, then secondary) sensors at XAN. The STS-2 1 sps channels were initially called LHZ, LHN, LHE, without a location code. After installation of the STS-1 on 1995.149 (149 representing the julian day), these channel names were used for the STS-1, and no LH data were recorded on the STS-2. On 1999.181, the STS-1 channels were renamed with the location code 00. We refer to these channels as LHZ-00, LHN-00, and LHE-00. LH data from the STS-2 sensor (location code 10) also recommenced on 1999.181 and we refer to these 1 sps channels as LHZ-10, LHN-10, and LHE-10. Epoch boundaries are given at 1992.334 (first STS-2 data), 1995.149 (first STS-1 data), and 1999.181 (current configuration). The metadata indicate no changes in gain or frequency characteristics of the two sensors during the period 1992–2009.

1.4 Scaling analysis

One method for assessing the quality of the data is the systematic comparison of recorded long-period waveforms with synthetic seismograms calculated for known seismic events. This analysis follows the steps described by Ekström et al. (2006). Seismic data for the LH and VH channels from both the STS-1 and STS-2 sensors are collected. Corresponding synthetic waveforms for all earthquakes in the Global CMT catalog (Dziewonski et al., 1981; Ekström et al., 2005) with $M_W \geq 6.5$ are calculated. Correlation coefficients and optimal scaling factors between observed and synthetic waveforms are calculated for the three types of data used in the standard CMT analysis: body waves (B), with periods in the range 50–150 sec, mantle waves (M), with periods in the range 125–350 sec, and surface waves (S), with periods in the range 50–150 sec. The scaling factor is only calculated for waveforms with a correlation of 0.75 or greater. The scaling factor is the number by which the synthetic seismogram should be multiplied to maximize the agreement with the observed seismogram. Annual median values of the scaling factors are calculated when four or more individual event scaling estimates are available for the year. Reversed components can be identified by their large negative correlations.

Figure 2 shows the results of our systematic comparison of XAN waveforms with synthetic seismograms. The diagram illustrates several problems with the data. Good correlation of all three components of the primary sensor with synthetic waveforms is only seen during 1995–1998. Starting in 1999, the horizontal components do not match the long-period synthetic waveforms. The vertical STS-1 began to deteriorate in 2005. The vertical and E-W components of the STS-2 appear to have started malfunctioning in 2008. In 2008 and 2009, of the six broadband components operating, only the STS-2 N-S channel recorded signals that agree with those predicted.

1.5 Noise analysis

A second method for investigating the overall performance of the sensors is to monitor background noise levels for all seismic channels, after conversion of the data to ground acceleration. We calculate hourly rms values of the time-domain seismic signal in narrow frequency bands, and convert the rms values to a power

spectral density (PSD) at that frequency using Parseval's theorem. For each month, we then calculate the low-noise value at each frequency by determining the PSD amplitude not exceeded 10% of the time.

The PSD data provide much information about the station and the sensors. Figure 3 shows the monthly low-noise estimate for each LH channel at 72 s period since 1992. The first observation is that the station has been providing data without major outages since 1992. From late 1994 through early 1995 there is a gap of several months. Second, the apparent noise levels have changed several times since 1992. A reduction in the noise is seen in 1995, associated with the change from the STS-2 to the STS-1 sensor. Vertical noise levels of the STS-2 are high in 1999, but then become similar to those of the STS-1. Horizontal noise levels of the STS-1 drop slightly in 1999, but this is probably associated with the loss of instrument gain (Figure 2). Vertical STS-1 noise levels are low and reasonable from 2000–2004.

At the end of 2004, noise levels increase and become highly erratic for some channels. Starting in 2008, the STS-1 vertical signal is extremely noisy, off scale in the plot. The STS-2 vertical component continued to record useful long-period earthquake signals through 2007 (Figure 2) in spite of increased noise levels.

1.6 Inter-sensor coherence

An additional method for assessing the quality and calibration of the recorded signals is to calculate inter-sensor coherence. This analysis is possible when more than one sensor is operated in the same location. At XAN, this is possible for the period 1999-2009, during which time both STS-1 and STS-2 instruments have been operating.

We calculate the coherence of the deconvolved vertical, N–S, and E–W components. The coherence is calculated for $\sim$2-hour-long time windows containing the signals for earthquakes with $M_W \geq 6.5$ (the same events used in the scaling analysis). For each pair of seismograms, the coherence is calculated in narrow frequency bands around 32 s, 64 s, 128 s and 256 s. If the coherence is greater than 0.95, the value is stored together with the complex scaling factor (represented here as a scaling factor and phase shift) that should be applied to the secondary-sensor data to bring the two time series into the best agreement. In the following, the discussion is based on the initial assumption that the secondary (STS-2) sensor is properly calibrated and that deviations from a scaling factor of 1.0 and a phase shift of 0° should be attributed to differences between the true and reported response functions of the primary (STS-1) sensor.

Figure 4 shows the results of the coherence analysis for the vertical component. Until mid-2000, the analysis yielded no high-coherence measurements. For the period 2001–2002, there is fairly good agreement between the two sensors, both in amplitude and in phase at all four periods. During 2003, the measurements at 256-s period start to deviate. The trend continues in 2004–2007, with gradual loss of gain at shorter periods as well, and a corresponding phase shift. A seasonal signal is also apparent. We interpret the deviations as problems with the STS-1, since the scaling analysis shows that the STS-2 signal remains in agreement with the synthetic signals through 2007 (Figure 2). A sudden step in the scaling factor is evident in late 2007 (Figure 2), and no coherence measurements are possible after early 2008.

Figure 5 shows the amplitude and phase differences for the N–S components. The agreement between the signals is never good during the period 1999–2009, with amplitude factors varying between 0.1 and 0.9 depending on the period and the time. The time variations are dramatic, showing mainly an annual periodicity, with the largest deviations in the late summer months of each year.

Figure 6 shows the results for the E–W component. Remarkably, the results are very similar to the N–S component, with a slightly smaller range of variations but with the same seasonal periodicity. Since the horizontal components of the STS-2 provide good scaling to the synthetic waveforms (Figure 2), we infer that the time-dependent differences should be attributed to the STS-1. However, since the horizontal

components originate from individual seismometers, it is not clear to us why the differences are so similar for the two components. In early 2008, an abrupt change in the inter-sensor scaling factor, but without a corresponding change in the phase, is attributable to some malfunction of the STS-2 also evident in Figure 2.

1.7 Polarization analysis

The orientation of the horizontal components can be assessed empirically by comparing observed and synthetic waveforms, and finding the angle by which the horizontal components should be rotated in order to maximize the agreement. We follow the approach described by Ekström and Busby (2008) for such a comparison, using the observed and synthetic waveforms from Global CMT analysis.

We apply the method of Ekström and Busby (2008) to the same dataset used in the scaling analysis. Figure 7 shows the individual measurements for the period of operation for the different channels. Overall, the number of useful observations for the STS-1 sensor is small, a consequence of the malfunctioning horizontal components. The STS-2 has generated more measurements, but the scatter of these measurements has been quite large, especially since 2008, probably a result of the sudden gain change on the N-S component seen in Figure 2. The median estimates for the entire period of operation are given in Table 1. In general, the median observations are consistent with the orientations provided in the metadata.

Comp. 1	Comp. 2	First	Last	# Obs.	N	Az 1	Az 2	25%	Med.	75%
LHE	LHN	19921220	19990517	233	49	90	0	-3	1	5
LHE-00	LHN-00	19990711	20090623	384	38	90	0	-6	4	9
LHE-10	LHN-10	19990711	20090623	385	109	90	0	-3	0	5

Table 1: Statistics of sensor-rotation angles estimated in this study. Columns are the channel names, the dates of the first and last observations considered in making the estimate, the total number of observations, the number of observations of acceptable quality, the reported azimuths of sensitivity of the two channels, the median polarization-angle deviation from the reported orientation together with the range of the second (25%) and third (75%) quartiles of the observations.

1.8 Example seismograms

The anomalies described here agree with observations we have made in our routine analysis of waveforms for the determination of CMT earthquake parameters. When confronted with the seismograms for an individual earthquake, it is often difficult to assess whether a poor fit is due to incorrect source parameters, inadequate modeling of wave propagation through an Earth model, or some problem with the recorded seismograms. Here, we have included some examples of data that illustrate the characteristics of the types of problems that we have encountered with data from the XAN station.

Figure 8 shows an example of three-component STS-1 mantle-wave data for an earthquake on February 2, 1998. All components are well fit, reflecting the general health of the station before 1999.

The top panel of Figure 9 shows a comparison between mantle-wave seismograms recorded on the STS-1 sensor and the corresponding synthetic waveforms for an event on December 6, 2000. By this date, both the amplitude and the phase of the waveforms are poorly matched on the horizontal components. The vertical component of the STS-1 is still functioning well. The bottom panel of Figure 9 shows the comparison between seismograms recorded on the STS-2 seismometer and the corresponding synthetic waveforms for the same event. For this sensor the fit is good for all components.

The top panel of Figure 10 shows a comparison of body-wave seismograms recorded on the STS-1 seismometer and the corresponding synthetic waveforms for an event on May 16, 2009. The vertical component is dead, and the horizontal components are grossly wrong. The bottom panel shows the STS-2 seismograms. The seismograms are similar to the synthetic waveforms, but the vertical and E-W amplitudes are significantly in error. One consequence of these errors is the poor result obtained when rotating the seismograms into transverse and longitudinal components (bottom pair of traces).

2 Summary and analysis

At the time of writing (January, 2010), the GSN station XAN is essentially broken. Only the N–S component of the secondary sensor is operating at, or close to, the expected quality. The functioning of the LHN-10 component is supported by the observation that both body- and mantle-wave waveforms are well fit by synthetics in the CMT analysis (Figure 2). No other component is demonstrably recording calibrated ground-motion data.

The horizontal STS-1 seismometers are malfunctioning and have been malfunctioning since at least 1999. The response is dramatically time dependent as well as frequency dependent. This is demonstrated best by the comparison with synthetic waveforms (Figure 2) and the coherence analysis (Figure 5 and Figure 6). The noise analysis is consistent with this, but is by itself not conclusive. In fact, based only on the data presented in Figure 3, one might conclude that horizontal noise levels have decreased since 1996. No useful data have been recorded by the horizontal STS-1 since 1999.

The deterioration of the STS-1 (Figures 4–6) shows a seasonal variability. This is similar to behavior reported in an earlier WQC report for station CASY-IU (Ekström and Nettles, WQC Report 2010:1).

The STS-2 sensor generated good data between 2000 and sometime early in 2008, although noise levels appear to have increased abruptly in 2004 (Figure 3). The vertical and E–W responses changed abruptly in 2007, without corresponding changes in the metadata, such that these components became severely uncalibrated.

3 Conclusions and recommendations

This analysis shows that XAN generated data of GSN quality only for a period of three years, 1996–1998. The station has suffered from a chronic sensor problem since 1999, a period of more than 10 years. Unfortunately, the highly erratic behavior of the horizontal components makes it unlikely that any retroactive remedy for the observed problem will be possible.

The sensor problems identified here should have been identified early on, and corrected. We speculate that the problem went unnoticed or undiagnosed because no routine calibrations are performed at GSN stations. The lack of systematic calibrations, and inspection of calibration results, makes it difficult to identify instrument problems. In addition, the lack of calibrations makes it nearly impossible to repair errors in instrument parameters once a problem has been identified. The symptoms of the STS-1 malfunction are similar to those observed at other stations (Ekström et al., 2006); interpretation is complicated by the presence of multiple sensor problems.

Modern seismological analyses require well-calibrated instruments. Amplitude variations of 10% and smaller are interpreted as signals in modern studies that seek to map the attenuating properties of the Earth's interior (e.g., Dalton and Ekström, 2006). Phase anomalies of a few seconds at long periods are similarly interpreted in terms of Earth's elastic structure by numerous authors. Data from XAN have been used in such studies with the assumption that the station is meeting GSN design goals (IRIS, 1985; Lay et al., 2002)

with respect to instrument stability. Clearly it does not, and its failure to do so should be documented. This is particularly important when, as for XAN, the data may at times appear visually to be correct, but are actually faulty.

It is urgent to restore XAN to a state where it generates GSN-quality data. It is especially unfortunate that the STS-2 has not provided quality replacement data during the last few years. It would be fruitful to determine the cause of the sudden loss of gain for the vertical and E–W STS-2 components. It is possible that a simple repair or STS-2 sensor replacement would restore baseline GSN functionality at the station.

4 References

Dalton, C. A., and G. Ekström, Global models of surface wave attenuation, *J. Geophys. Res.*, 111, B05317, 2006.

Dziewonski, A. M., T.-A. Chou, and J. H. Woodhouse, Determination of earthquake source parameters from waveform data for studies of global and regional seismicity, *J. Geophys. Res.*, 86, 2825–2853, 1981.

Ekström, G., A. M. Dziewonski, N. N. Maternovskaya, and M. Nettles, Global seismicity of 2003: Centroid-moment tensor solutions for 1087 earthquakes, *Phys. Earth Planet. Inter.*, 148, 327–351, 2005.

Ekström, G., C. A. Dalton, and M. Nettles, Observations of time-dependent errors in long-period gain at global seismic stations, *Seism. Res. Lett.*, 77, 12–22, 2006.

Ekström, G., and R. W. Busby, Measurements of seismometer orientation at USArray Transportable and Backbone stations, *Seism. Res. Lett.*, 79, 554-561, 2008.

Ekström, G., and M. Nettles, Performance of the GSN station CASY-IU, 1996–2009, Waveform Quality Center Report 2010:1, 2010.

IRIS, *The design goals for a new global seismographic network*, IRIS GSN committee report, 31 pages, 1985.

Lay, T., J. Berger, R. Buland, R. Butler, G. Ekström, B. Hutt, B. Romanowicz, *Global seismic network design goals update 2002*, IRIS GSN committee report, 2002.

Nettles, M., and G. Ekström, Glacial earthquakes in Greenland and Antarctica, *Annual Reviews*, in review, 2010.

Peterson, J., Observations and modeling of background seismic noise, *U. S. Geol. Surv. Open-file Rep. 93-322*, 1–45, 1993.

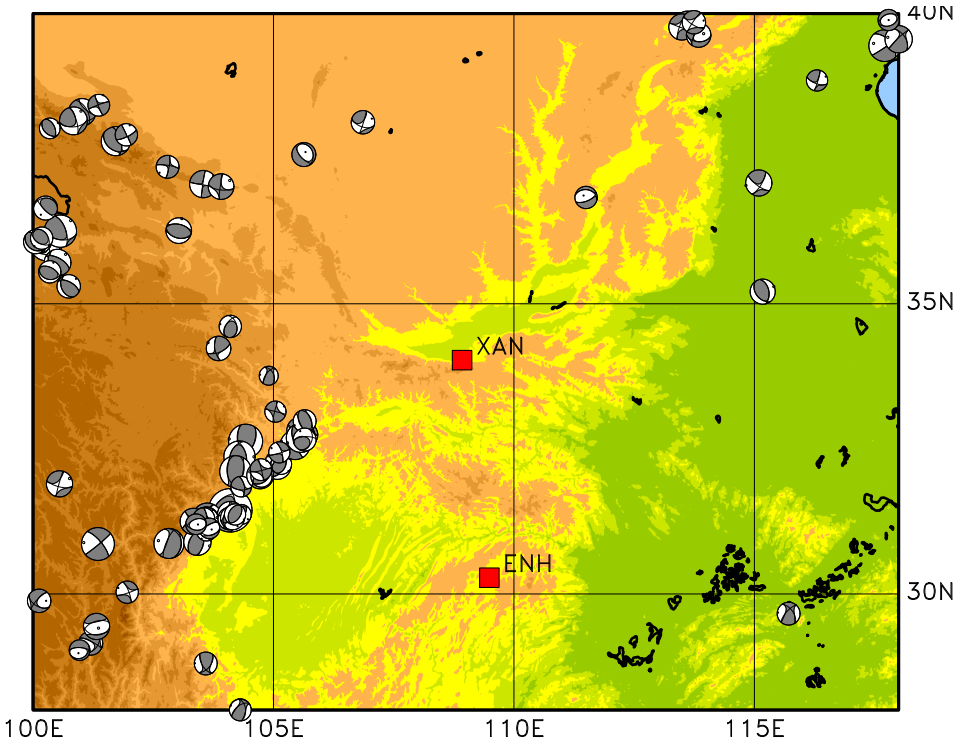

Figure 1: Map showing the location of XAN (red square in the center). Grey focal mechanisms show locations and moment tensors from the Global CMT catalog. The dense linear cluster of focal mechanisms to the southwest of the station corresponds to the earthquake sequence following the $M_W = 7.9$ Sichuan earthquake on May 12, 2008. The closest GSN and FDSN station is ENH-IC, shown with the red square towards the bottom of the map.

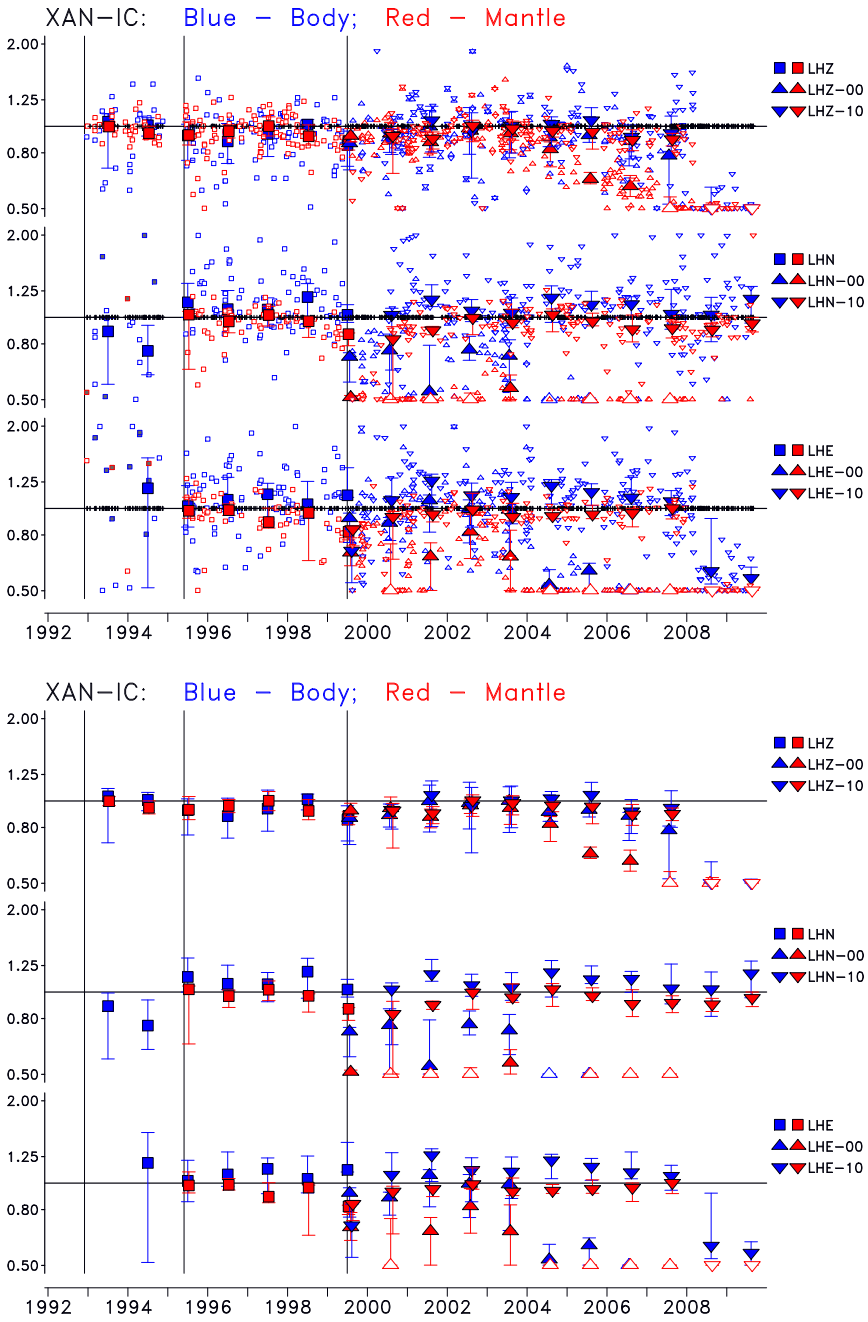

Figure 2: Scaling factors for the different data channels at XAN. Small symbols in top panel show scaling factors for individual traces. Tick marks on the horizontal axes show times of observations for which the correlation was less than 0.75. Large symbols show the median scaling factor for each year, with the error bars corresponding to the range of the second and third quartiles of the scaling factors. The legend on the right identifies the symbol type with a specific channel. Open large symbols indicate that the annual scaling factor was smaller than 0.5. Thin vertical lines show the response epoch boundaries present in the metadata. Bottom panel shows only the annual median values.

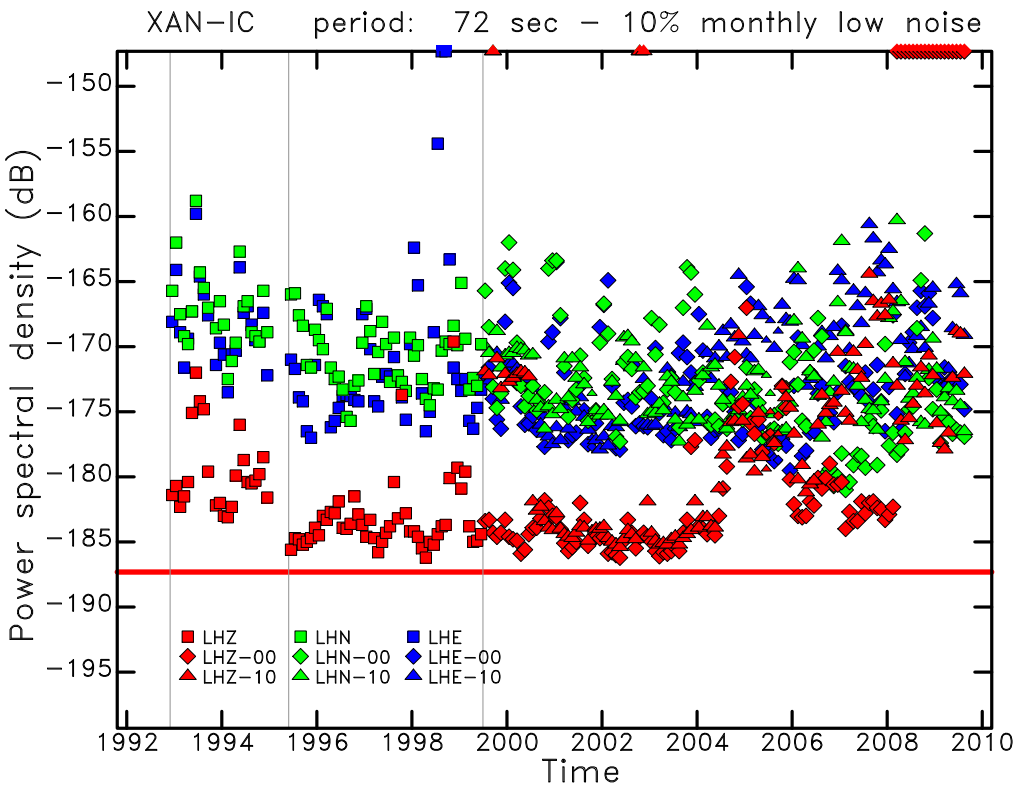

Figure 3: Diagram shows the monthly PSD of ground acceleration at 72-s period for all long-period (LH) channels at XAN for the period 1988–2009. Smaller symbols are used for months with fewer available hourly measurements. Each component and sensor is represented by a distinct symbol and color. The red horizontal line indicates the level of Peterson's (1993) Low Noise Model (LNM) at 72 s. The thin vertical lines show the times of epoch boundaries in the station metadata.

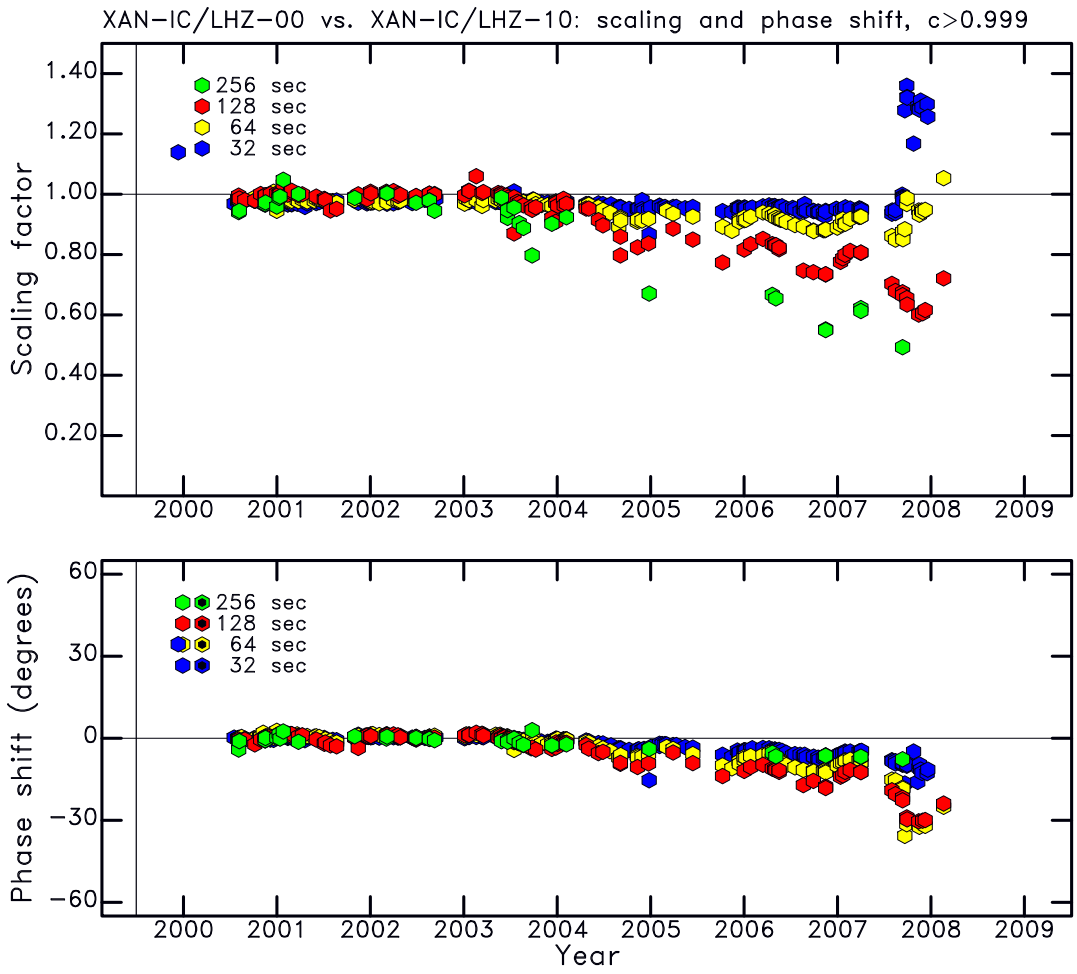

Figure 4: Diagram shows the result of the coherence analysis for the vertical components of the STS-1 and STS-2 sensors. Each symbol represents a measurement of coherence for a $M_W \geq 6.5$ earthquake. The minimum coherence plotted is indicated by c. The scaling and phase between the two time series is shown at four different periods. Starting in 2003, the long-period response of the STS-1 begins to deteriorate. The STS-1 vertical failed in 2008. The thin vertical lines show the times of epoch boundaries in the station metadata.

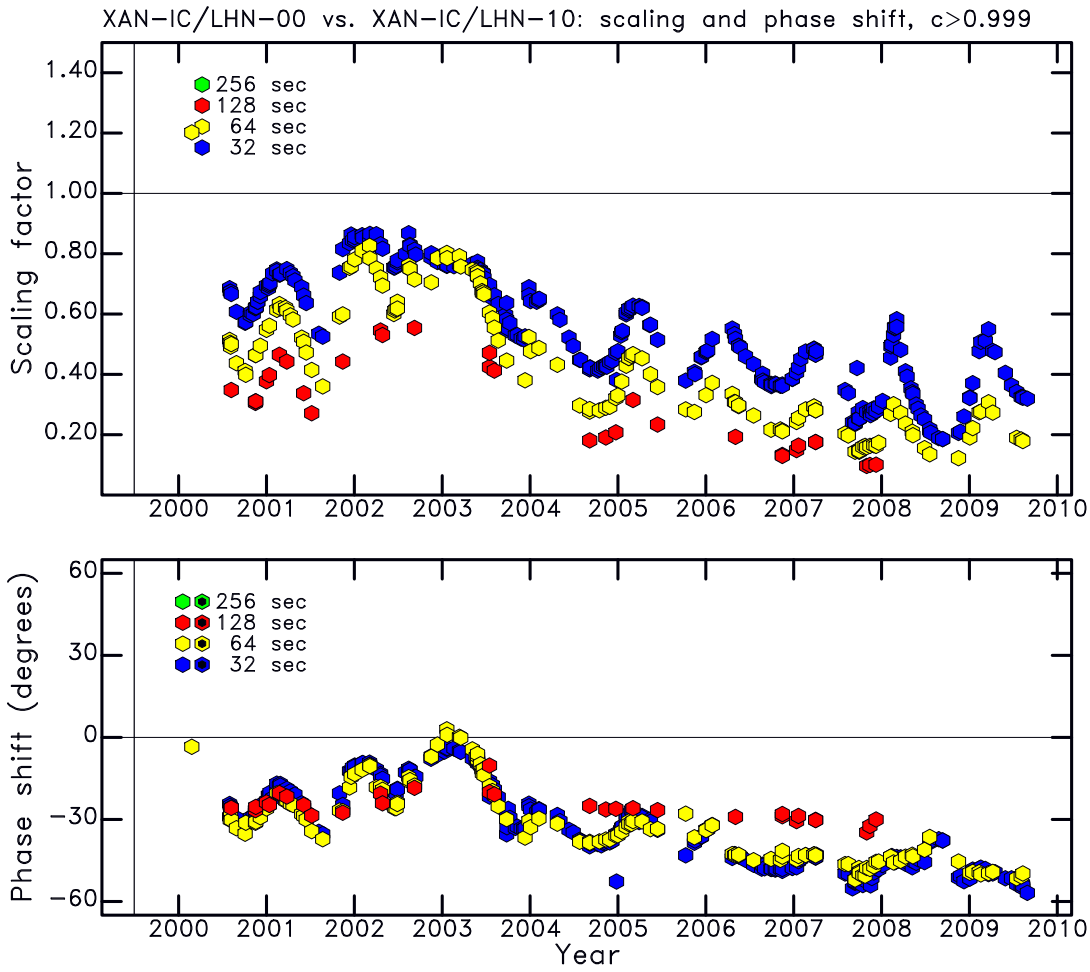

Figure 5: Same as Figure 4, but for the North-South components. Very large, frequency-dependent and time-varying differences in the amplitude and the phase between the signals from the STS-1 and STS-2 sensors are seen during the entire period. The variations have a clear seasonality, with the largest deviations during the late boreal summer.

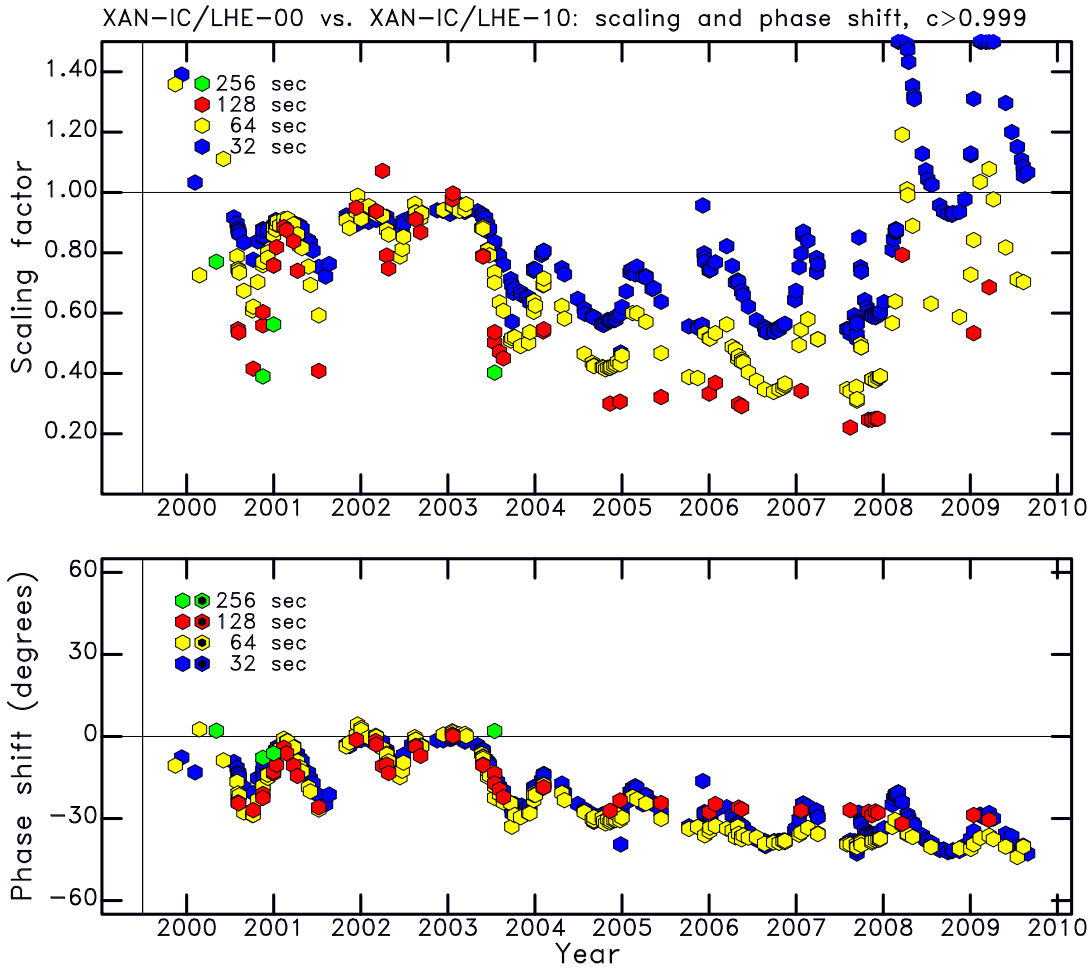

Figure 6: Same as Figure 4, but for the East-West components. The problems on the East-West component are similar to those on the North-South component, except for an additional step-like change in 2008 which can be attributed to a failure of the STS-2 component, also evident in Figure 2.

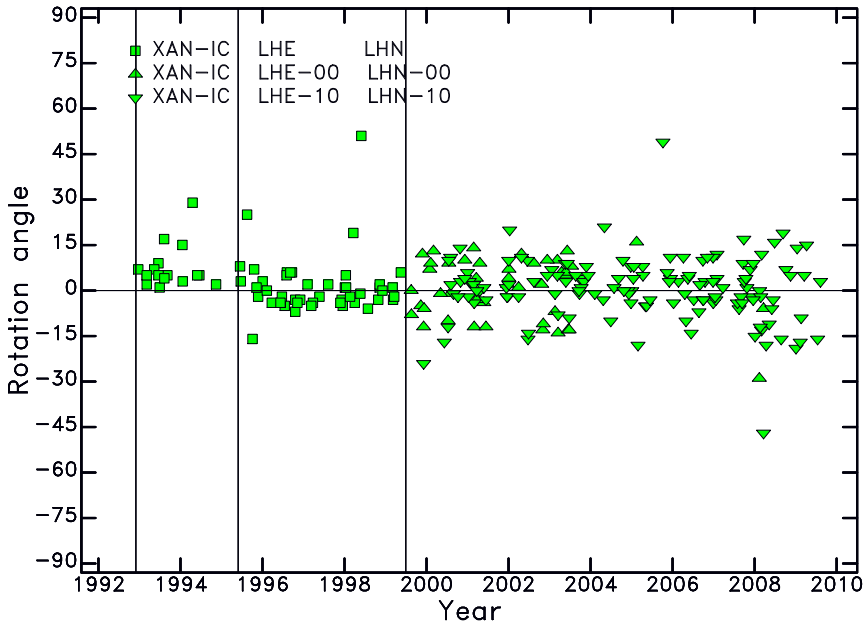

Figure 7: Individual measurements of polarization angle as a function of time. All measurements for the period of operation are shown. Symbols represent measurements obtained in the surface-wave band of the CMT analysis. The thin vertical lines show the times of epoch boundaries in the station metadata.

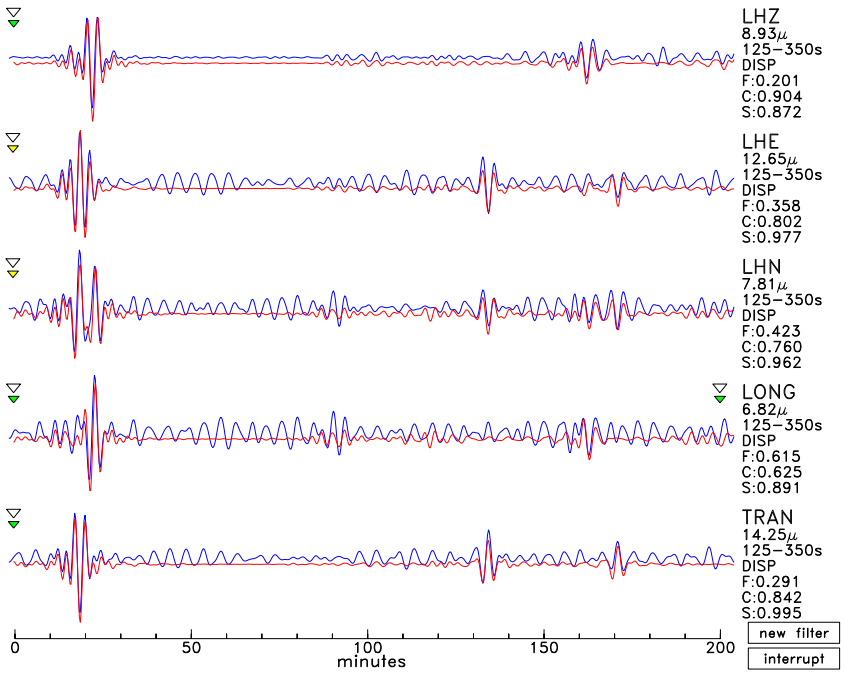

Figure 8: Comparison of observed (blue traces) and synthetic (red traces) mantle-wave seismograms recorded on the STS-1 sensor for an earthquake on February 2, 1998. The channel name, maximum displacement, and values for the three parameters residual misfit (F), correlation (C) and scaling factor (S) are given to the right of each waveform. All channels are well fit.

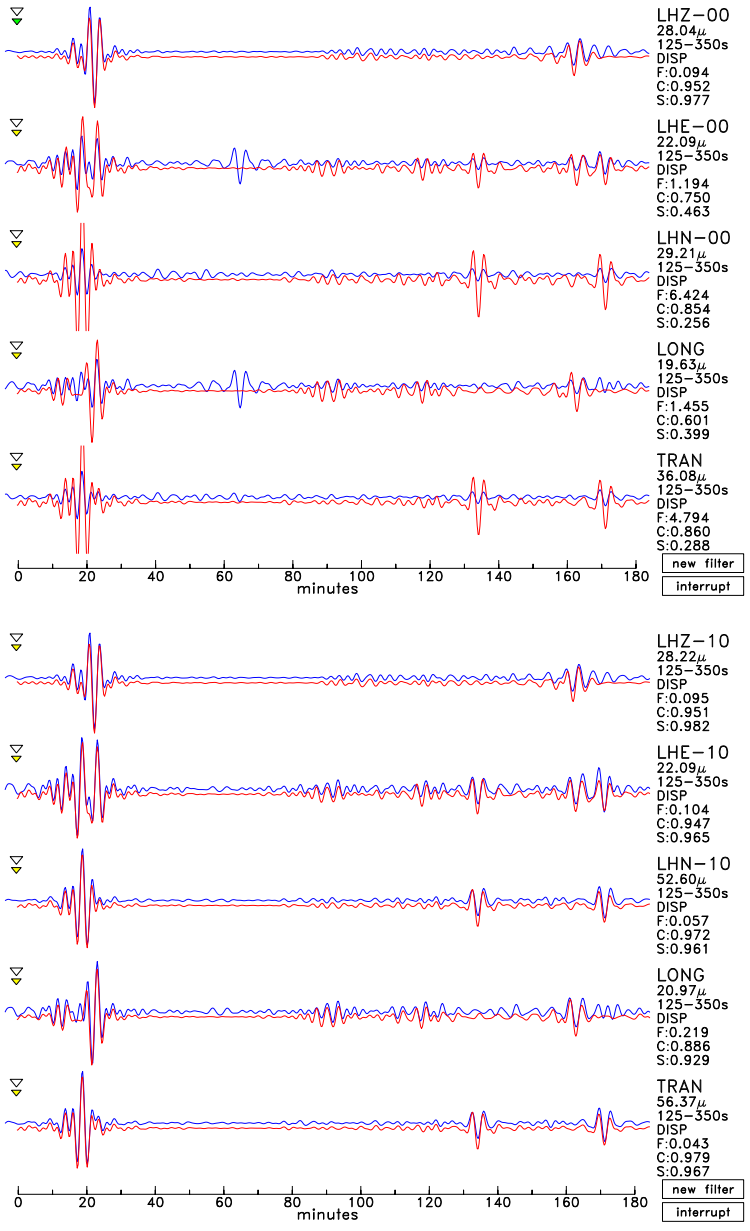

Figure 9: (Top) Observed (STS-1) and synthetic mantle-wave seismograms for an earthquake on December 6, 2000. The East–West and N–S components are poorly fit, reflecting errors in the response functions. The problem is not only a difference in gain. (Bottom) Observed (STS-2) and synthetic body-wave seismograms for the same earthquake, but recorded on the STS-2 seismometer. The fit to all three components is good.

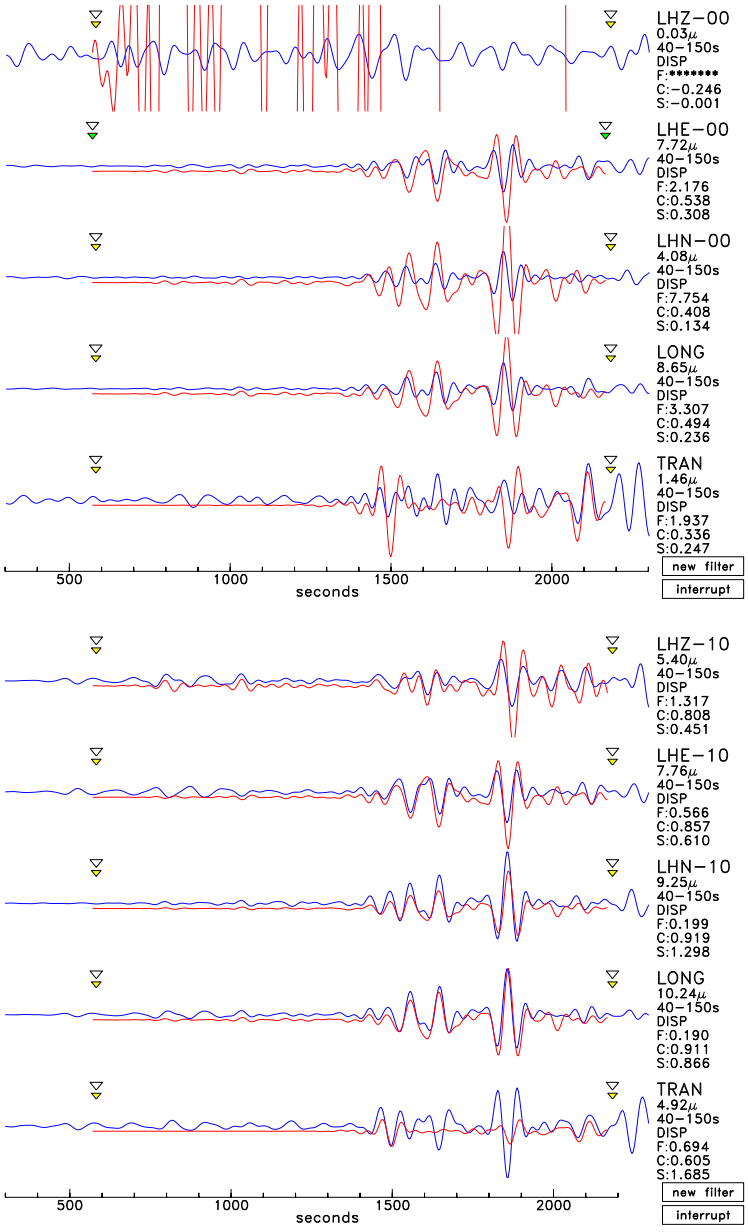

Figure 10: (Top) Observed (STS-1) and synthetic body-wave seismograms for an earthquake on May 16, 2009. The vertical component is dead. The horizontal components are uncalibrated. The problem is not only a difference in gain. (Bottom) Observed (STS-2) and synthetic body-wave seismograms for the same earthquake, but recorded on the STS-2 seismometer. The fit is poor on the vertical and E–W components.